Optimized Schwarz methods with an overset grid for the shallow-water equations: preliminary results

Qaddouri, Abdessamad; Laayouni, Lahcen; Loisel, Sébastien; Côté, Jean; Gander, Martin Jakob

How to cite

QADDOURI, Abdessamad et al. Optimized Schwarz methods with an overset grid for the shallow-water equations: preliminary results. In: Applied numerical mathematics, 2008, vol. 58, n° 4, p. 459–471. doi: 10.1016/j.apnum.2007.01.015

This publication URL: https://archive-ouverte.unige.ch/unige:6266
Publication DOI: 10.1016/j.apnum.2007.01.015

Optimized Schwarz methods with an overset grid for the shallow-water equations: preliminary results

Abdessamad Qaddouri [a,1,2], Lahcen Laayouni [b,1], Sébastien Loisel [c,1], Jean Côté [a,1,2] and Martin J. Gander [c,1]

[a] *Recherche en prévision numérique, Environnement Canada, Dorval, Canada*

[b] *Department of Mathematics and Statistics, McGill University, Montréal, Canada*

[c] *Section de Mathématiques, Université de Genève, Genève, Switzerland*

Abstract

The overset grid nicknamed "Yin-Yang" grid is singularity free and has quasi-uniform grid spacing. It is composed of two identical latitude/longitude orthogonal grid panels that are combined to cover the sphere with partial overlap on their boundaries. The system of shallow-water equations (SWEs) is a hyperbolic system at the core of many models of the atmosphere. In this paper, the SWEs are solved on the Yin-Yang grid by using an implicit and semi-Lagrangian discretization on a staggered mesh. The resulting scalar elliptic equation is solved using a Schwarz-type domain decomposition method, known as the optimized Schwarz method, which gives better performance than the classical Schwarz method by using specific Robin or higher order transmission conditions.

Key words: optimized Schwarz methods, Yin-Yang grid, shallow-water equations, domain decomposition

1 Introduction

We use a domain decomposition method to solve the system of shallow-water equations (SWEs) using the Yin-Yang grid on the sphere. In this grid system the globe is partitioned into two identical

Email addresses: Abdessamad.qaddouri@ec.gc.ca (Abdessamad Qaddouri), laayouni@math.mcgill.ca (Lahcen Laayouni), loisel@math.unige.ch (S´ebastien Loisel), jean.cote@ec.gc.ca (Jean Côt´e), gander@math.unige.ch (Martin J. Gander).

[1] Partially supported by the Canadian Foundation for Climate Atmospheric Science

[2] Partially supported by U.S. Department of Energy

latitude/longitude orthogonal grid panels that are combined to cover the sphere with partial overlap on their boundaries, and we consider the hyperbolic problem in each subdomain over a given time interval and using the same time step.

The local solver is the same fully implicit semi-Lagrangian method as in the GEM operational model [1]: uniform Arakawa staggered C-Grid, 2-time-level iterative semi-Lagrangian scheme with in time interpolated advecting wind, iterative non-linear solver for the positive definite Helmholtz problem, iterative treatment of the Coriolis terms by grouping them with non-linear terms, and metric terms using the Lagrange multiplier approach [2]. We use the semi-Lagrangian time discretization scheme in spherical coordinates to approximate the Lagrangian derivative along particle trajectories defined by the velocity field. A finite-volume method is used for the spatial discretization. This discretization is implemented independently on each quasi-uniform lat/long part grid. The trajectories are computed for each grid panel in 3D Cartesian geometry with the restriction that the trajectories are confined to the surface of the sphere. We adopt the two-time scheme to evaluate a field on a trajectory. The value at an upstream point is determined by the cubic Lagrange interpolation either in the Yin (if this point is in Yin) or the Yang grid panel.

The implicit treatment of the terms responsible for gravity waves in the SWEs gives rise to a 2d elliptic boundary value problem that must be solved at each time step. We use here a domain decomposition method, where the solution of the global elliptic problem is obtained by iteratively solving the corresponding two subproblems separately on the Yin and the Yang grids, and updating the values at the interfaces. In recent years, much attention has been given to domain decomposition methods for solving linear elliptic problems that are based on a partitioning of the domain of the physical problem. The initial idea of the Schwarz method was given by Schwarz [3] as a method for proving existence and uniqueness of solutions in irregular domains for the Laplace equation. The method is now used as an iterative method in modern applied mathematics, see for example Quarteroni and Valli [4]. The classical alternating Schwarz method consists of solving iteratively subdomain problems and using the subdomain solutions to update the interface conditions of neighboring subdomains. Because the two subgrids of the Yin-Yang grid do not match, the update is done by cubic Lagrange interpolation and this corresponds to Dirichlet interface condition. To improve the performance of the classical domain decomposition methods we use optimized Schwarz methods, see Gander [6] and references therein.

The paper is organized as follows: in Section 2, we present the model formulation, in Section 3 the various Schwarz methods, in Section 4 numerical results and finally concluding remarks in Section 5.

2 Formulation

In this section we briefly review the basic ideas of the semi-Lagrangian implicit solver.

2.1 Governing equations and time discretization

The governing equations on each (Yin or Yang) subgrid are the shallow-water equations on a rotating sphere of radius a. The implicit semi-Lagrangian time discretization proceeds as in Yeh et al. [1], and is $O(\Delta t^2)$ accurate. The resulting equation for the unknowns U, V, the wind images [wind divided by $a\ cos\theta$], and ϕ the perturbation geopotential from the reference geopotential ϕ^* at forecast time t are

$$\left[\frac{U}{\tau} - fV + \frac{1}{a^2}\frac{\partial \phi}{\partial \lambda}\right](\lambda,\theta,t) = R_U, \tag{1}$$

$$\left[\frac{V}{\tau} + fU + \frac{1}{a^2}\cos\theta\frac{\partial \phi}{\partial \theta}\right](\lambda,\theta,t) = R_V, \tag{2}$$

$$\left[\frac{\phi^* \ln(1+\frac{\phi}{\phi^*})}{\tau} + \phi^* D\right](\lambda,\theta,t) = R_\phi, \tag{3}$$

where

$$R_U = \left[\frac{U}{\tau} + fV - \frac{1}{a^2}\frac{\partial \phi}{\partial \lambda}\right]\left(\lambda^-,\theta^-,t-\Delta t\right) + \delta_m U, \tag{4}$$

$$R_V = \left[\frac{V}{\tau} - fU - \frac{1}{a^2}\cos\theta\frac{\partial \phi}{\partial \theta}\right]\left(\lambda^-,\theta^-,t-\Delta t\right) + \delta_m V, \tag{5}$$

$$R_\phi = \left[\frac{\phi^* \ln(1+\frac{\phi}{\phi^*})}{\tau} - \phi^* D\right]\left(\lambda^-,\theta^-,t-\Delta t\right), \tag{6}$$

and D and f are the divergence and Coriolis parameter respectively and are defined by

$$D = \frac{1}{\cos^2\theta}\left(\frac{\partial U}{\partial \lambda} + \cos\theta\frac{\partial V}{\partial \theta}\right), \qquad f = 2\Omega\sin\theta. \tag{7}$$

Here Ω is the angular speed of the Earth's rotation and λ^-, θ^- are the upstream longitude and latitude at time $t-\Delta t$ of the fluid element arriving at the grid point λ, θ at the forecast time t, $\tau = \Delta t/2$ and $\delta_m U$ and $\delta_m V$ are the metric corrections terms computed following C$\hat{}$ot´e [2].

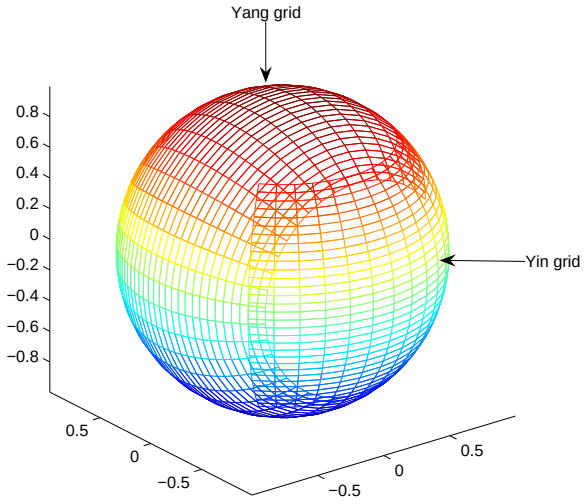

Fig. 1. The Yin-Yang grid system.

In the two time-level semi-Lagrangian discretization we need to estimate the trajectories of the fluid elements. On the sphere the trajectories are great circles whose parameters, for centered schemes, are determined by the winds at time $t - \tau$ calculated by linear interpolation of the wind vector. In (1)-(3), the value of the various fields at an upstream point is determined by cubic Lagrange interpolation in either the Yin or the Yang grid panel.

2.2 Spatial discretization

The Yin-Yang grid in its most basic shape is shown in Fig. 1. It has two grid components which are geometrically identical. They are combined to cover a spherical surface with partial overlap on their borders. Each component is in fact a part of the latitude-longitude grid: each component grid is defined in spherical polar coordinates by

$$(-\frac{\pi}{4} - \delta_\theta \leq \theta \leq \frac{\pi}{4} + \delta_\theta) \cap (-\frac{3\pi}{4} - \delta_\lambda \leq \lambda \leq \frac{3\pi}{4} + \delta_\lambda), \tag{8}$$

where $\delta_\lambda, \delta_\theta$ are small buffers, which are proportional to the respective grid-spacings, required for a minimum overlap in the overset methodology. A uniform cell-integrated finite-volume discretization on a staggered Arakawa C grid is used for each subgrid to discretize equations (1)-(3). This means the arrival points at time t for U, V and ϕ are all staggered with respect to one another. For uniform resolution, this becomes the usual staggered finite difference formulation.

The right-hand sides R_U and R_V in (1) and (2) are first interpolated to the scalar grid using 1d cubic Lagrange interpolation. The results denoted by R_U^s and R_V^s, where the superscript s refers to

the scalar grid, are then interpolated at the upstream position λ^-, θ^-. Next, the metric correction terms $\delta_m U^s$ and $\delta_m V^s$ are added, on the scalar grid, to ensure that horizontal displacements are spherically constrained

$$(\Delta R_U^s; \Delta R_V^s) = \left(R_U^s(\lambda^-, \theta^-) + \delta_m U^s - R_U^s(\lambda, \theta); R_V^s(\lambda^-, \theta^-) + \delta_m V^s - R_V^s(\lambda, \theta) \right). \quad (9)$$

The increments ΔR_U^s and ΔR_V^s are then interpolated back to U and V grids, respectively, using 1d cubic Lagrange interpolation and the results denoted by ΔR_U^u and ΔR_V^v to be added to the starting values at grid points to get the final right-hand sides R_U and R_V.

2.3 A model time step

For each subdomain, a Crank-Nicolson iteration then consists of

(1) computation of the trajectories,
(2) computation of the right hand sides of the momentum and continuity equations without metric effects,
(3) interpolation to the upstream point,
(4) inclusion of the metric effects,
(5) computation of the right hand side of the positive definite Helmholtz equation and iterative solution with communication of the geopotential,
(6) updating of the wind.

In practice we perform 2 Crank-Nicolson iterations per time step and 2 iterations in the non-linear Helmholtz problem solver.

3 Optimized Schwarz method

In this Section, we first show that the shallow-water equations with implicit time discretization lead to a sequence of positive definite Helmholtz problems which can be solved by domain decomposition methods. We then analyze the convergence of Schwarz domain decomposition methods with Dirichlet and Robin transmission conditions for positive definite Helmholtz problems in 1d. Finally, we present second-order transmission conditions for the 2d positive definite Helmholtz problem on the sphere with two subdomains corresponding to the Yin-Yang grid.

3.1 1d linear shallow-water equations

The governing equations are the 1d linear shallow-water equations on the circle $[0, 2\pi]$. This domain is divided into two overlapping subdomains. We show that the periodic solutions (ϕ and u) of the SWEs can be obtained by updating the geopotential in the two subdomains with an optimized Schwarz method. The global solution can also be recovered when the two subdomain (scalar) grids do not match and even when there is no overlap. The generalization to 2d is straightforward.

We have chosen subdomains of identical size, but other cases could be analyzed as well. We use N grid points for the scalar (ϕ-grid) and $N-1$ grid points for the wind (u-grid) in both angular subdomains $\Omega_1 = [0, \pi+\delta]$ and $\Omega_2 = [\pi, 2\pi+\delta]$, where δ is the overlap. The discretized equations on each subdomain Ω_l, $l = 1, 2$ are

$$\frac{u_i^{(l)}}{\tau} + \frac{1}{a}\frac{\phi_{i+1}^{(l)} - \phi_i^{(l)}}{h} = R_{u\,i}^{(l)}, \quad i = 1, \ldots, N-1, \tag{10}$$

$$\frac{\phi_i^{(l)}}{\tau} + \frac{\phi^*}{a}\frac{u_i^{(l)} - u_{i-1}^{(l)}}{h} = R_{\phi\,i}^{(l)}, \quad i = 1, \ldots, N, \tag{11}$$

where ϕ^* is a positive constant and

$$\begin{aligned} R_{u\,i}^{(l)} &= \frac{u_i^{-(l)}}{\tau} - \frac{1}{a}\frac{\phi_{i+1}^{-(l)} - \phi_i^{-(l)}}{h}, \quad i = 1, \ldots, N-1, \\ R_{\phi\,i}^{(l)} &= \frac{\phi_i^{-(l)}}{\tau} - \frac{\phi^*}{a}\frac{u_i^{-(l)} - u_{i-1}^{-(l)}}{h}, \quad i = 1, \ldots, N. \end{aligned} \tag{12}$$

If the grids match, and this is the case analyzed here, then $\delta = n_\delta h$ is a multiple of the angular grid spacing h. Periodicity, continuity and uniqueness imply

$$\begin{aligned} &\phi_1^{(1)} = \phi_{N-n_\delta}^{(2)},\ \phi_N^{(1)} = \phi_{1+n_\delta}^{(2)},\ \phi_0^{(1)} = \phi_{N-n_\delta-1}^{(2)},\ \phi_{N+1}^{(1)} = \phi_{2+n_\delta}^{(2)}, \\ &u_0^{(1)} = u_{N-n_\delta-1}^{(2)},\ u_N^{(1)} = u_{1+n_\delta}^{(2)}. \end{aligned} \tag{13}$$

Given fields at the previous time step ($u^{-(l)}$ and $\phi^{-(l)}$), the two subdomains calculate in parallel their right-hand-sides $R_u^{(l)}$ and $R_\phi^{(l)}$. Extra communication is necessary at initial time ($u_0^{(l)}$,$u_N^{(l)}$,$\phi_0^{(l)}$,$\phi_{N+1}^{(l)}$) to calculate extended right-hand-sides $R_{u\,0}^{(l)}$ and $R_{u\,N}^{(l)}$ using (12). By subtracting Eq. (10) expressed at two neighboring points $i-1$ and i we have

$$\frac{u_i^{(l)} - u_{i-1}^{(l)}}{a\tau h} + \frac{1}{a^2}\frac{\phi_{i+1}^{(l)} - 2\phi_i^{(l)} + \phi_{i-1}^{(l)}}{h^2} = \frac{R_{u\,i}^{(l)} - R_{u\,i-1}^{(l)}}{ah}, \quad i = 1, \ldots, N-1. \tag{14}$$

This latter equation is used with Eq. (11) in order to eliminate $u^{(l)}$ and to obtain the discretized elliptic equation for $\phi^{(l)}$ which we solve iteratively with iteration index $k = 1, \ldots, k_{max}$ in each subdomain,

$$\frac{-\phi_{i+1}^{(l),k} + 2\phi_i^{(l),k} - \phi_{i-1}^{(l),k}}{h^2} + \eta\phi_i^{(l),k} = R_{H\,i}^{(l)}, \quad i = 1, \ldots, N, \tag{15}$$

where

$$R_{H\,i}^{(l)} = \frac{a^2 R_{\phi\,i}^{(l)}}{\tau\phi^*} - \frac{a(R_{u\,i}^{(l)} - R_{u\,i-1}^{(l)})}{h}, \quad \eta = \frac{a^2}{\tau^2\phi^*}. \tag{16}$$

For each subdomain Ω_l, $l = 1, 2$, we use at the subdomain boundaries the transmission conditions

$$\begin{aligned} \frac{\phi_2^{(l),k} - \phi_0^{(l),k}}{2h} + \beta_1^{(l)}\phi_1^{(l),k} = b_1^{(l),k} &= \frac{\phi_{N+1}^{(3-l),k-1} - \phi_{N-1}^{(3-l),k-1}}{2h} + \beta_1^{(l)}\phi_N^{(3-l),k-1}, \\ \frac{\phi_{N+1}^{(l),k} - \phi_{N-1}^{(l),k}}{2h} + \beta_2^{(l)}\phi_N^{(l),k} = b_2^{(l),k} &= \frac{\phi_2^{(3-l),k-1} - \phi_0^{(3-l),k-1}}{2h} + \beta_2^{(l)}\phi_1^{(3-l),k-1}. \end{aligned} \tag{17}$$

We use the discretized elliptic equation (15) and the transmission conditions (17) in order to eliminate from the subdomain Ω_l equations the unavailable values $\phi_0^{(l),k}$ and $\phi_{N+1}^{(l),k}$ that are in subdomain Ω_{3-l} at the current time step. The 4 scalars $\beta_i^{(l)}$ are chosen to optimize the convergence rate of the Schwarz method and are precomputed analytically. The system (15-17) is solved iteratively with the initial values provided by the values $\phi^{-(l)}$ of the previous time step.

After the elliptic solver we have an extended updated vector of geopotential $[\phi_0^{(l),k_{max}}, \phi_1^{(l),k_{max}}, \ldots, \phi_N^{(l),k_{max}}, \phi_{N+1}^{(l),k_{max}}]$ in each subdomain. The two subdomains can update an extended vector of wind $u^{(l)}$ in parallel

$$u_i^{(l)} = \tau\left(R_{u\,i}^{(l)} - \frac{1}{a}\frac{\phi_{i+1}^{(l),k_{max}} - \phi_i^{(l),k_{max}}}{h}\right), \quad i = 0, \ldots, N. \tag{18}$$

These become the past values for the next time step, and all the needed information is local and only $b_1^{(l),k}$ and $b_2^{(l),k}$ of (17) need to be exchanged at the level of the Schwarz method.

3.2 Convergence analysis for the periodic 1d positive definite Helmholtz problem

We now study the convergence of the Schwarz method at the continuous level, using closed form solutions in each subdomain. The novelty here is in the periodicity of the global domain and solution. The sphere is periodic in any direction and the impact of periodicity needs to be studied before the iterative Schwarz methods are applied to the Yin-Yang grid.

3.2.1 Iterative solution at the continuous level

To find iteratively a periodic solution of the positive definite Helmholtz problem on the circle,

$$(\eta - \partial_{\lambda\lambda})\phi = R \quad \text{on} \quad \Omega = [0, 2\pi], \quad \eta > 0, \tag{19}$$

we decompose the circle Ω into two overlapping subdomains

$$\Omega_1 = [0, \pi + \delta], \quad \Omega_2 = [\pi, 2\pi + \delta], \quad \text{with} \quad \Omega = \Omega_1 \cup \Omega_2, \tag{20}$$

and use an optimized Schwarz iteration of the form

$$\begin{aligned}
(\eta - \partial_{\lambda\lambda})\phi^{(1),k} &= R^{(1)} \quad \text{on } \Omega_1, & (\eta - \partial_{\lambda\lambda})\phi^{(2),k} &= R^{(2)} \quad \text{on } \Omega_2, \\
B_1^{(1)}\phi^{(1),k}(0) &= B_1^{(1)}\phi^{(2),k-1}(2\pi), & B_1^{(2)}\phi^{(2),k}(\pi) &= B_1^{(2)}\phi^{(1),k-1}(\pi), \\
B_2^{(1)}\phi^{(1),k}(\pi + \delta) &= B_2^{(1)}\phi^{(2),k-1}(\pi + \delta), & B_2^{(2)}\phi^{(2),k}(2\pi + \delta) &= B_2^{(2)}\phi^{(1),k-1}(\delta),
\end{aligned} \tag{21}$$

where the $B_i^{(l)}$ are interface operators to be specified in each subdomain Ω_l, $l = 1, 2$, and which can involve derivatives of ϕ. In practice, they depend on parameters that are chosen to accelerate the convergence of the iterative process. To analyze the convergence of iteration (21), we use on each subdomain at iteration k the closed form solution

$$\phi^{(l),k}(\lambda) = a^{(l),k}e^{\kappa\lambda} + b^{(l),k}e^{-\kappa\lambda} = \begin{bmatrix} e^{\kappa\lambda} & e^{-\kappa\lambda} \end{bmatrix} \begin{bmatrix} a^{(l),k} \\ b^{(l),k} \end{bmatrix}, \tag{22}$$

where $\kappa = \sqrt{\eta}$ and the coefficients $a^{(l),k}$, $b^{(l),k}$ are determined by the transmission conditions from the previous iteration. The matrix relation between the coefficients at 2 consecutive iterations is the transition matrix whose spectral radius (eigenvalue of greatest modulus) determines the

convergence rate of the iterative process. To simplify the following development, we introduce the interface locations $\lambda_i^{(l)}$ of each subdomain and their images $\widetilde{\lambda}_i^{(l)}$ in the other subdomain, i.e.,

$$\begin{aligned} &\lambda_1^{(1)} = 0, \quad \lambda_2^{(1)} = \pi + \delta, \quad \lambda_1^{(2)} = \pi, \quad \lambda_2^{(2)} = 2\pi + \delta, \\ &\widetilde{\lambda}_1^{(1)} = 2\pi, \quad \widetilde{\lambda}_2^{(1)} = \pi + \delta, \quad \widetilde{\lambda}_1^{(2)} = \pi, \quad \widetilde{\lambda}_2^{(2)} = \delta. \end{aligned} \tag{23}$$

With this notation, the transmission conditions in (21) become

$$\begin{aligned} B_1^{(l)}\phi^{(l),k}(\lambda_1^{(l)}) &= B_1^{(l)}\phi^{(3-l),k-1}(\widetilde{\lambda}_1^{(l)}), \\ B_2^{(l)}\phi^{(l),k}(\lambda_2^{(l)}) &= B_2^{(l)}\phi^{(3-l),k-1}(\widetilde{\lambda}_2^{(l)}). \end{aligned} \tag{24}$$

Rewriting this relation in matrix form using the closed form solutions (22), we get

$$\mathbf{M}_{(l)} \begin{bmatrix} a^{(l),k} \\ b^{(l),k} \end{bmatrix} = \widetilde{\mathbf{M}}_{(l)} \begin{bmatrix} a^{(3-l),k-1} \\ b^{(3-l),k-1} \end{bmatrix}, \tag{25}$$

where the matrices are given by

$$\mathbf{M}_{(l)} = \begin{bmatrix} B_1^{(l)} e^{\kappa\lambda_1^{(l)}} & B_1^{(l)} e^{-\kappa\lambda_1^{(l)}} \\ B_2^{(l)} e^{\kappa\lambda_2^{(l)}} & B_2^{(l)} e^{-\kappa\lambda_2^{(l)}} \end{bmatrix}, \qquad \widetilde{\mathbf{M}}_{(l)} = \begin{bmatrix} B_1^{(l)} e^{\kappa\widetilde{\lambda}_1^{(l)}} & B_1^{(l)} e^{-\kappa\widetilde{\lambda}_1^{(l)}} \\ B_2^{(l)} e^{\kappa\widetilde{\lambda}_2^{(l)}} & B_2^{(l)} e^{-\kappa\widetilde{\lambda}_2^{(l)}} \end{bmatrix}. \tag{26}$$

The transition matrix is then obtained by considering the 2 subdomains simultaneously

$$\mathbf{T} = \begin{bmatrix} 0 & \mathbf{M}_{(1)}^{-1}\widetilde{\mathbf{M}}_{(1)} \\ \mathbf{M}_{(2)}^{-1}\widetilde{\mathbf{M}}_{(2)} & 0 \end{bmatrix}. \tag{27}$$

Considering a double iteration, T^2 has the same eigenvalues as the reduced 2×2 iteration matrix

$$\mathbf{A}(k,\delta) = \mathbf{M}_{(1)}^{-1}\widetilde{\mathbf{M}}_{(1)}\mathbf{M}_{(2)}^{-1}\widetilde{\mathbf{M}}_{(2)}. \tag{28}$$

3.2.2 Classical Schwarz method

By choosing the $B_i^{(l)}$ to be equal to the identity in (21), we obtain the classical Schwarz method. This means that each subdomain is providing as boundary condition to the other the solution on

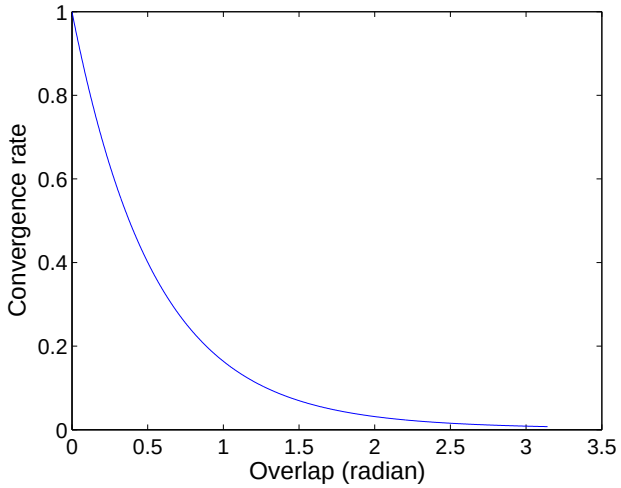

Fig. 2. Convergence factor of the classical Schwarz method for overlap δ varying from 0 to π and fixed $\kappa = \sqrt{\eta} = 1$.

its domain. The convergence factor obtained from (28) is then

$$\rho_{\text{classical Schwarz}}(\kappa,\delta) = \frac{\left(e^{\kappa\pi} + e^{\kappa\delta}\right)^2}{\left(1 + e^{\kappa(\pi+\delta)}\right)^2}, \quad \text{and} \quad \begin{cases} \rho_{\text{classical Schwarz}} = 1 \text{ if } \delta = 0, \\ \rho_{\text{classical Schwarz}} < 1 \text{ if } \delta > 0. \end{cases} \tag{29}$$

Fig. 2 shows the convergence factor of the classical Schwarz method for the overlap δ varying from 0 to π with κ set to 1. There is a lack of convergence for zero overlap and slow convergence for practical overlap greater than zero but small. For these reasons, the classical Schwarz method is in general used as a preconditioner in preconditioned Krylov methods and rarely as an iterative solver by itself.

3.2.3 Optimized Schwarz method with Robin transmission conditions

The slow convergence of the classical Schwarz method motivates the development of optimized Schwarz methods which run at the same or at little extra cost. The improvement comes from changing the transmission conditions to include derivatives. The general form of the transmission conditions then depends on parameters that can be chosen to optimize the convergence rate. The extra cost is in the determination of the optimized parameters, but they can be precomputed once and for all for a given geometry and problem setting.

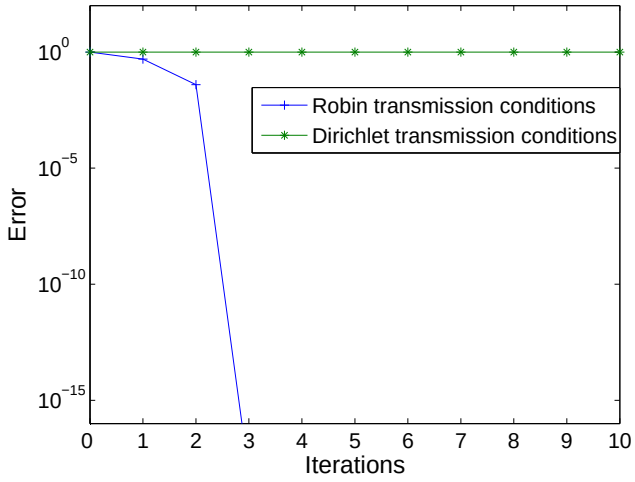

Fig. 3. Convergence behavior of the classical Schwarz and the optimized Schwarz method with Robin transmission conditions for the 1d positive definite Helmholtz equation, overlap $\delta = 0$ and $\kappa = \sqrt{\eta} = 1$.

We consider here transmission operators of the form

$$B_i^{(l)} = \partial_\lambda + \beta_i^{(l)}, \tag{30}$$

where the $\beta_i^{(l)}$ are real constants to be determined. In this case the analysis is more involved, but as before, the convergence factor is obtained by computing the spectral radius of $\mathbf{A}$. We find

$$\mathbf{M}_{(l)} = \begin{bmatrix} (\beta_1^{(l)} + \kappa)e^{\kappa\lambda_1^{(l)}} & (\beta_1^{(l)} - \kappa)e^{-\kappa\lambda_1^{(l)}} \\ (\beta_2^{(l)} + \kappa)e^{\kappa\lambda_2^{(l)}} & (\beta_2^{(l)} - \kappa)e^{-\kappa\lambda_2^{(l)}} \end{bmatrix}, \quad \widetilde{\mathbf{M}}_{(l)} = \begin{bmatrix} (\beta_1^{(l)} + \kappa)e^{\kappa\widetilde{\lambda}_1^{(l)}} & (\beta_1^{(l)} - \kappa)e^{-\kappa\widetilde{\lambda}_1^{(l)}} \\ (\beta_2^{(l)} + \kappa)e^{\kappa\widetilde{\lambda}_2^{(l)}} & (\beta_2^{(l)} - \kappa)e^{-\kappa\widetilde{\lambda}_2^{(l)}} \end{bmatrix} \tag{31}$$

$$\rho_{\text{Optimized Robin}}(\kappa, \delta) = \min_{\beta_1^{(1)}, \beta_2^{(1)}, \beta_1^{(2)}, \beta_2^{(2)}} \rho\left(\mathbf{A}\left(\kappa, \delta; \beta_1^{(1)}, \beta_2^{(1)}, \beta_1^{(2)}, \beta_2^{(2)}\right)\right).$$

This optimization problem can be solved analytically, giving $\rho = 0$. The optimized Robin coefficients obtained are $\beta_1^{(1)} = -\kappa \tanh(\kappa(\frac{(\pi-\delta)}{2}))$, $\beta_2^{(1)} = -\beta_1^{(1)}$, $\beta_1^{(2)} = -\kappa \coth(\kappa(\frac{(\pi-\delta)}{2}))$, and $\beta_2^{(2)} = -\beta_1^{(2)}$. Fig. 3 illustrates how the use of Robin transmission conditions with the optimal coefficients above leads to an iterative method where the maximum error vanishes in the third iteration. The first iteration is needed to compute solutions of the subdomain problems in both subdomains that correspond to some arbitrary initial guess at the interfaces. The two following iterations are then required for the error to vanish, according to (30), which implies that with the optimal choice, the iteration matrix $\mathbf{A}$ vanishes identically. It is interesting to note that for the periodic problem, three iterations are needed with the optimal choice to obtain the exact solution, whereas for non-periodic problems, two iterations suffice.

3.3 Optimized Schwarz method for 2d positive definite Helmholtz problems on the sphere

By eliminating the wind components U and V from the shallow-water equations on the sphere, we obtain a positive definite Helmholtz equation for the geopotential ϕ,

$$\mathcal{L}\phi = \eta\phi - \Delta\phi = R, \quad \text{in } S \subset \mathbb{R}^3, \tag{32}$$

where S stands for the unit sphere centered at the origin, η is the same positive parameter given in (16), and R is the corresponding right-hand-side function.

We decompose the sphere into two overlapping domains as shown in Fig. 1. On each grid we use local spherical coordinates, with constant radial direction, and we rewrite the positive definite Helmholtz problem in the form

$$\mathcal{L}\phi = \eta\phi - \frac{1}{\cos^2(\theta)}\frac{\partial^2\phi}{\partial\lambda^2} - \frac{\partial^2\phi}{\partial\theta^2} + \tan\theta\frac{\partial\phi}{\partial\theta} = R. \tag{33}$$

Similar to the 1d case, we solve iteratively in each subdomain the discretized problems

$$\begin{aligned}\eta\phi_{i,j}^{(l),k} - \frac{1}{\cos^2\theta_j}\frac{\phi_{i+1,j}^{(l),k} - 2\phi_{i,j}^{(l),k} + \phi_{i-1,j}^{(l),k}}{h_\lambda^2} - \frac{\phi_{i,j+1}^{(l),k} - 2\phi_{i,j}^{(l),k} + \phi_{i,j-1}^{(l),k}}{h_\theta^2} \\ + \tan\theta_j\frac{\phi_{i,j+1}^{(l),k} - \phi_{i,j-1}^{(l),k}}{2h_\theta} = R_{i,j}^{(l),k}, \quad i = 1,\ldots,N;\ j = 1,\ldots,M,\end{aligned} \tag{34}$$

where h_λ, h_θ are the grid spacings and N, M the grid-point numbers along the longitudinal and latitudinal direction respectively. Collecting terms in (34) leads to

$$\begin{aligned}-\frac{2 + h_\theta\tan\theta_j}{2h_\theta^2}\phi_{i,j-1}^{(l),k} - \frac{1}{\cos^2\theta_j h_\lambda^2}\phi_{i-1,j}^{(l),k} + (\eta + \frac{2}{\cos^2\theta_j h_\lambda^2} + \frac{2}{h_\theta^2})\phi_{i,j}^{(l),k} \\ -\frac{1}{\cos^2\theta_j h_\lambda^2}\phi_{i+1,j}^{(l),k} - \frac{2 - h_\theta\tan\theta_j}{2h_\theta^2}\phi_{i,j+1}^{(l),k} = R_{i,j}^{(l),k}, \quad i = 1,\ldots,N;\ j = 1,\ldots,M.\end{aligned} \tag{35}$$

Following ideas in Gander [6],we use on the interfaces between the subdomains discretizations of the higher order transmission conditions

$$\frac{\partial\phi^{(l),k}}{\partial\nu_l} + \beta_d^{(l)}\phi^{(l),k} + \alpha_d^{(l)}\frac{\partial^2\phi^{(l),k}}{\partial\tau_l^2} = \frac{\partial\phi^{(3-l),k-1}}{\partial\nu_l} + \beta_d^{(l)}\phi^{(3-l),k-1} + \alpha_d^{(l)}\frac{\partial^2\phi^{(3-l),k-1}}{\partial\tau_l^2} \text{ on } \Gamma_d^{(l)}, \tag{36}$$

where $\Gamma_d^{(l)}$ $(d = 1 \cdots 4)$ are the boundaries on the panel l of the Yin-Yang grid and $\alpha_d^{(l)}$ and $\beta_d^{(l)}$ are real parameters introduced to optimize the performance of the method. The symbol $\frac{\partial}{\partial \nu_l}$ stands for the normal derivative of each subdomain and $\frac{\partial}{\partial \tau_l}$ is the corresponding tangential derivative. Note that when all $\beta_d^{(l)}$ go to infinity, while the $\alpha_d^{(l)}$ stay bounded, we recover the classical Schwarz method, which is known for its weakness to handle the lowest modes and its slow convergence. Setting $\alpha_d^{(l)} = 0$, for all d and l, we obtain the Schwarz method with Robin transmission conditions, for which we need to find the optimal parameters $\beta_d^{(l)}$ to obtain best performance. The second-order Schwarz method corresponds to the case when the $\alpha_d^{(l)}$ are not necessarily zero. We have obtained these coefficients numerically assuming the coefficients $\alpha_d^{(l)}$ and $\beta_d^{(l)}$ are equal in both subdomains, i.e.

$$\alpha_d^{(1)} = \alpha_d^{(2)}, \quad \beta_d^{(1)} = \beta_d^{(2)}, \tag{37}$$

where moreover the coefficients are assumed to be independent of the boundary d. For those approximate optimal values of the parameters $\alpha_d^{(l)}$ and $\beta_d^{(l)}$ the corresponding methods converge in a small number of iterations and the convergence is much better than the convergence of the classical Schwarz method. This gain more than compensates for the extra cost of computing the needed additional derivatives. Furthermore, the optimized Schwarz methods converge even without overlap between subdomains, while the classical Schwarz method stagnates in that case. Having a small overlap however between subdomains further improves the performance of the optimized Schwarz methods.

4 Numerical Results

We illustrate now the above developments by numerical results. We first present 1d linear results to show that the experimental results are in agreement with the theoretical prediction. Next we present passive advection and the elliptic solver in 2d. We have not yet validated the full 2d shallow-water model on the Yin-Yang grid but the necessary elements of advection and the elliptic solver have been thoroughly tested.

4.1 Linear 1d shallow-water equations on a circle

We perform numerical experiments for our linear SWEs model problem on the circle $[0,\ 2\pi]$. The initial conditions are

$$\begin{aligned} u(\lambda) &= A_u \cos(k\lambda) + C_u \sin(k\lambda), \\ \phi(\lambda) &= A_\phi \cos(k\lambda) + C_\phi \sin(k\lambda); \quad \lambda \in [0, 2\pi], \end{aligned} \tag{38}$$

where the integer wave number $k = 20$ and the amplitudes $A_u = 20m/s$, $C_u = 20m/s$, $A_\phi = 10m^2/s^2$ and $C_\phi = 10m^2/s^2$ are real, $\phi^* = 5000 \times 9.80616m^2/s^2$, and $a = 6.37122e^6m$. The angular domain $[0, 2\pi]$ is decomposed into two non overlapping subdomains $\Omega_1 = [0, \pi]$ and $\Omega_2 = [\pi, 2\pi]$. We use a Crank-Nicolson discretization in time and a finite-volume discretization in space in each subdomain, with a time step Δt of 2 hours and uniform angular mesh parameter h equal to $\pi/100$. We compare the numerical solution against the exact discrete solution given by

$$\begin{aligned} u(\lambda, t) &= A_u \cos(k\lambda)\cos(\omega t) + B_u \cos(k\lambda)\sin(\omega t) + C_u \sin(k\lambda)\cos(\omega t) + D_u \sin(k\lambda)\sin(\omega t) \\ \phi(\lambda, t) &= A_\phi \cos(l\lambda)\cos(\omega t) + B_\phi \cos(k\lambda)\sin(\omega t) + C_\phi \sin(k\lambda)\cos(\omega t) + D_\phi \sin(k\lambda)\sin(\omega t), \end{aligned} \tag{39}$$

where the amplitudes are

$$B_u = -\frac{C_\phi}{\sqrt{\phi^*}},\ D_u = \frac{A_\phi}{\sqrt{\phi^*}},\ B_\phi = -\sqrt{\phi^*}C_u,\ D_\phi = \sqrt{\phi^*}A_u, \tag{40}$$

and the frequency is given by

$$\omega = \frac{1}{\tau}\arctan\left(\tau k \frac{\sqrt{\phi^*}}{a}\frac{\sin(hk/2)}{hk/2}\right), \quad \tau = \Delta t/2. \tag{41}$$

For the values of the earth radius a, the time step Δt and the reference geopotential ϕ^* given above, we compute $\eta = 63.88$ using (16). The coefficients used in the optimized Robin transmission conditions are precomputed for this η, as shown in Sub-subsection 3.2.3, and are found to be $\beta_1^{(1)} = -7.992$, $\beta_2^{(1)} = -\beta_1^{(1)}$, $\beta_1^{(2)} = -7.992$ and $\beta_2^{(2)} = -\beta_1^{(2)}$. For this η, the analytic expressions of the coefficients happen to give the same numerical values in both subdomains. We simulate the evolution of linear SWEs over a period of 48 hours. The numerical geopotential against the exact discretized geopotential at the end of the simulation on domain Ω_1 are displayed in Fig. 4, the same kind of results are obtained on Ω_2. We present in Fig. 5 the difference between the numerical and the exact discretized geopotential perturbation (respectively wind) at the end of the

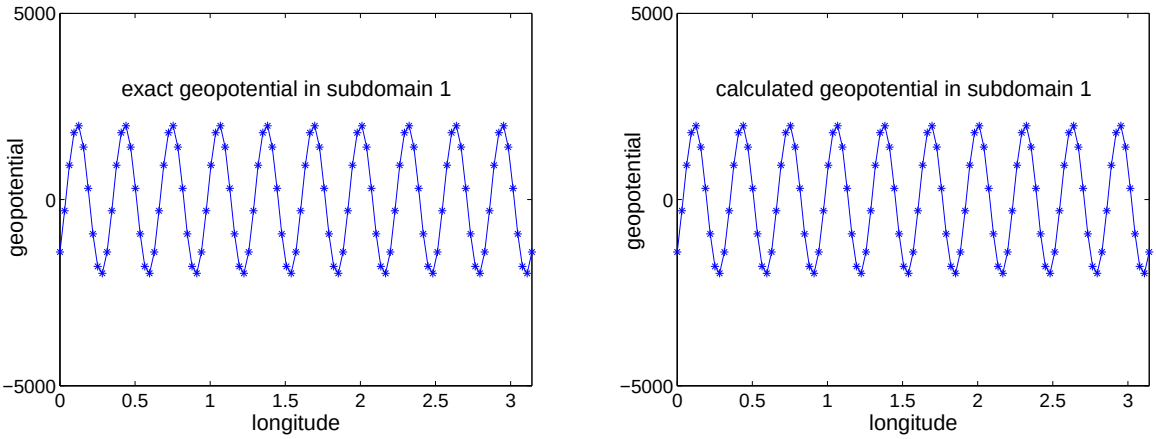

Fig. 4. Exact discretized and calculated geopotential on Domain Ω_1 for the SWEs after 48 hours .

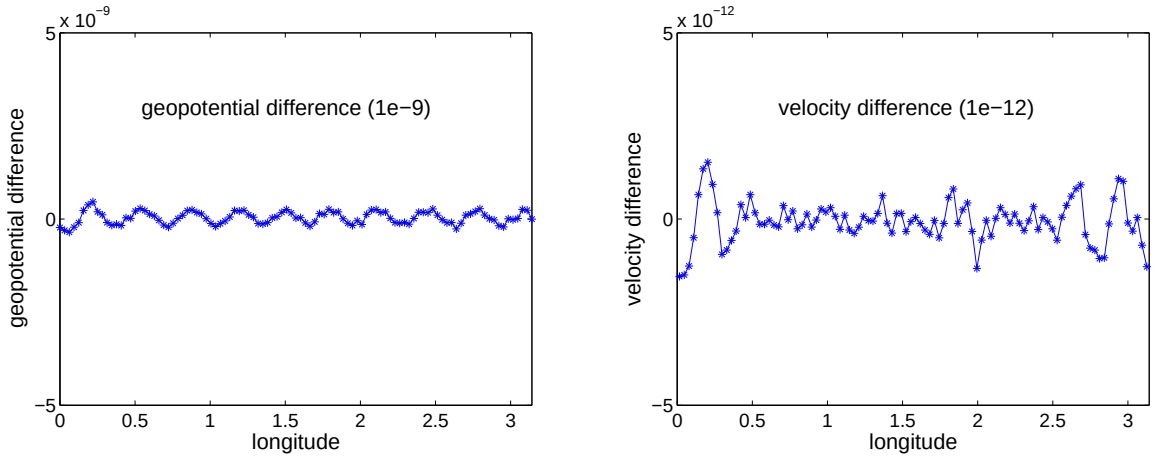

Fig. 5. Error in calculated geopotential and calculated velocity on Domain Ω_1 for the SWEs after 48 hours .

simulation. The difference should be 0 at full convergence of the iterative process. It is shown that the global exact discretized periodic solution for the linear 1d SWEs is obtained by the above domain decomposition where the local solutions are not periodic. This is obtained by doing only a few communications between the two subdomains in the iterative domain decomposition solver. We note that because the 2d grids we consider are tensor products of 1d grids, the generalization of the strategy of eliminating the wind in favor of solving only a distributed elliptic problem for the geopotential to 2d is straightforward.

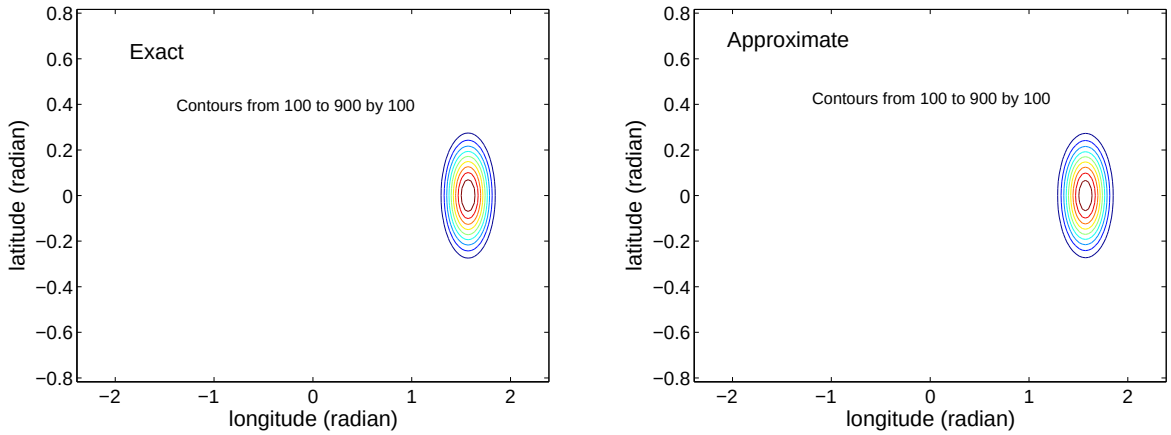

Fig. 6. Advection of the cosine bell in the Yin-Yang grid.

4.2 2d advection on the Yin-Yang grid

We consider the "cosine bell" test problem proposed by Williamson et al. [5]. This problem is widely used to test discretizations of the global advection equation

$$\left[\frac{\partial}{\partial t}+\frac{U}{\cos^2\theta}\frac{\partial}{\partial\lambda}+\frac{V}{\cos\theta}\frac{\partial}{\partial\theta}\right]F(\lambda,\theta,t)=0. \tag{42}$$

The initial scalar distribution is defined by

$$F(\lambda,\theta,0)=\begin{cases}F_0\dfrac{1+\cos(\pi r/R)}{2} & \text{if } r<R,\\ 0 & \text{if } r\geq R,\end{cases} \tag{43}$$

where $R=a/3$, $F_0=1000m$ and r is the great circle distance between (λ,θ) and the center of the scalar distribution (λ_c,θ_c),

$$r=a\arccos\left[\sin\theta_c\sin\theta+\cos\theta_c\cos\theta\cos(\lambda-\lambda_c)\right]. \tag{44}$$

The advecting wind is given by

$$\begin{aligned}u&=+u_0(\cos\theta\cos\alpha+\cos\lambda\sin\theta\sin\alpha),\\ v&=-u_0\sin\lambda\sin\alpha,\end{aligned} \tag{45}$$

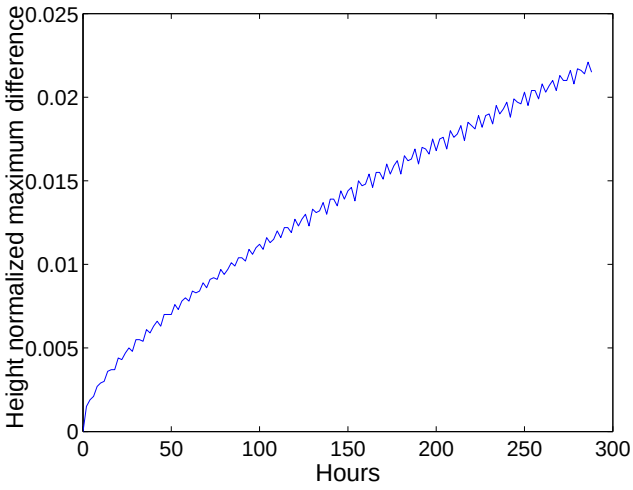

Fig. 7. Evolution of the normalized maximum difference during one revolution.

where the wind speed is $u_0 = 2\pi/T$, $T = 12$ days which is equivalent to about $40m/s$, and α is the orientation of the advecting wind. This solution should rotate without any change of shape. We use the semi-Lagrangian time discretization in spherical coordinates to approximate the Lagrangian derivative in (42) along the trajectories defined by the velocity field as in Cˆot´e and Staniforth [9]. The trajectories are calculated for each grid panel (Yin and Yang) in the three dimensional Cartesian geometry with the restriction that the trajectories are confined to the surface of the sphere. The value of the scalar field at an upstream point is determined by cubic Lagrange interpolation either in the Yin or the Yang grid panel. We ran two tests, where the above cosine bell is advected once around the sphere with the orientations $\alpha = 0$ and $\pi/2$. Since the Yin-Yang grid is pole free, these two tests are equivalent. The simulations are carried out with the resolution of 150×50 on both the Yin and the Yang grid, which is equivalent to a global horizontal resolution of $200km$. A time step of two hours is used, and it requires 144 time steps (288 hours) to rotate the cosine bell one full revolution around the Earth. Fig. 6 shows that there is no distortion in the shape of the bell at the end of the simulation. The bell structure is maintained in the Yin-Yang grid even where the bell passes trough the overlapped region. The time evolution of the normalized infinite error norm is presented in Fig. 7, and as can be seen the trend and the norm are comparable to those in Jacob-Chien et al. [7], and the norm after 12 days remains small and is equal 2%.

4.3 2d positive definite Helmholtz problem on the Yin-Yang grid

We perform now numerical experiments for the positive definite Helmholtz equation (32) on the surface of the sphere. We decompose the surface using the Yin-Yang grid, where each panel is discretized with a uniform grid of spacing h_λ, h_θ along the longitudinal and latitudinal direction

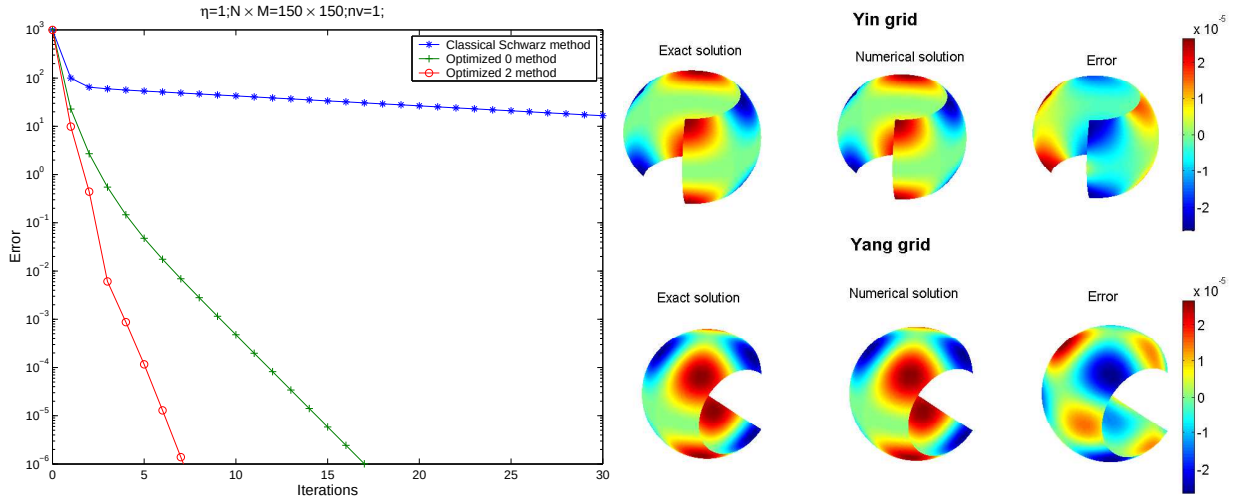

Fig. 8. **Left:** Convergence behavior for the methods analyzed for the two subdomains case. **Right:** Screen-shots of solutions and the error in the Yin-Yang grid.

respectively and we use the same number of grid-points in both directions, i.e., $N = M$. The overlap between the two subgrids is controlled by the buffer parameters δ_λ and δ_θ that are proportional to the grid-spacing in each direction. The two panels of the Yin-Yang grid cannot have a zero overlap throughout because of the geometry, but they can have very small overlap at some boundaries when δ_λ and δ_θ are small. We chose a right-hand-side in (32) so that the global solution on the surface of the sphere is

$$\phi(\lambda, \theta) = \cos^2\theta \sin^2\theta \sin\lambda \cos\lambda. \tag{46}$$

We use the finite difference scheme with five points given in (35) with the transmission conditions in (36). For the optimized Schwarz method with Robin transmission conditions (i.e., $\alpha_d^{(l)} = 0$) in the Yin-Yang grid, the best values of $\beta_d^{(l)}$ are evaluated numerically. To this end, we vary the coefficient $\beta_d^{(l)}$, supposed to be independent of the boundary, for a fixed $N = 150$ and count the number of iterations to obtain a relative residual of $1e^{-6}$. The best values of $\beta_d^{(l)}$ are found to be $\beta_d^{(1)} = \beta_d^{(2)} = -1.4$. Similarly the optimized values (Optimized 2) for Schwarz method with second order transmission conditions are evaluated numerically and are

$$\beta_d^{(1)} = \beta_d^{(2)} = -0.925, \qquad \alpha_d^{(1)} = \alpha_d^{(2)} = -0.085. \tag{47}$$

Fig. 8 shows a comparison between the number of iterations of the classical Schwarz method and the optimized ones for $\eta = 1$ $N = 150$ and the overlap (δ_λ and δ_θ) are at least one grid-spacing, to reach a relative residual of $1e^{-6}$. This figure shows, as we expected, how tremendously the optimized Schwarz methods improve the behavior of the classical Schwarz method when they are

	Classical Schwarz		Taylor 0 method		Taylor 2 method		Optimized 0 method	
h	$L = 1/50$	$L = h$	$L = 1/50$	$L = h$	$L = 1/50$	$L = h$	$L = 1/50$	$L = h$
1/50	184	184	22	22	16	16	12	12
1/100	184	284	22	27	16	19	12	16
1/150	183	389	21	31	15	21	11	19
1/200	184	497	22	36	16	24	12	22

Table 1
Number of iterations of the classical Schwarz method compared to the optimized Schwarz methods for the Yin-Yang grid system with $\eta = 1$.

used as iterative solvers. We also compare the classical Schwarz method and the above optimized Schwarz methods to zeroth and second order Taylor Schwarz methods (Cˆot´e et al., [8]). These methods use a low frequency expansion (about 0) of the optimal parameters which are obtained through Fourier analysis. In Table 1, we vary the grid-spacing and we compare the number of iterations of each method. We consider two situations: one with constant overlap $L = \pi/50$, and the other one with varying overlap $L = h$, (h_λ or h_θ), where L here measures the size of the smallest region between the two panels of the Yin-Yang grid. When the overlap is maintained constant, all the aforementioned methods converge independently of the grid size h. This is a well known property of the classical Schwarz method, but it does not mean that the classical Schwarz method is optimal: also the zeroth and second order Taylor Schwarz methods and the optimized Schwarz methods have the same property, but with an order of magnitude less iterations, and this at the same cost per iteration. In Fig. 8, we present some screen-shots of the numerical solutions computed with the second order optimized Schwarz method compared to the exact solutions in the two panels of the Yin-Yang grid.

5 Conclusion

In this paper, we have examined the application of Schwarz domain decomposition methods (DDM) to the solution of the shallow-water equations (SWEs) in the context of atmospheric modeling with a new horizontal grid nicknamed "Yin-Yang". We have first examined the linear SWEs in 1d. We have considered a periodic global domain and local non-periodic subdomains and solutions. It was shown that the optimized Schwarz method allowed us to recover the periodic solution of the linear SWEs with high accuracy. The convergence analysis of the 1d optimized Schwarz method yielded a practical formula for the optimized coefficients in the transmission conditions. The 2d case of the elliptic solver on the sphere for the Yin-Yang grid was treated numerically. We have shown that specific transmission conditions based on a linear combination of the function, its normal and second-order tangential derivatives yielded a dramatic improvement of the conver-

gence rates. The use of optimized Schwarz methods on the Yin-Yang grid is new. We have not yet validated the full 2d SWEs model on the Yin-Yang grid, but 2d passive semi-Lagrangian advection has been thoroughly tested for this grid. The 2d semi-Lagrangian advection scheme maintains the bell structure in the Yin-Ying grid even when the bell passes through the overlap region, and the distribution goes from one panel to the other. The normalized maximum error remains very small even after 12 days of evolution. In future work, we will complete the validation of the SWEs with the Yin-Yang grid using a real data case (case number 7) of Williamson et al. [5]. We will also study how to accelerate optimized Schwarz methods with Krylov methods, like it is done for classical Schwarz methods in general. Finally, an interesting and more involved question is the extension of the present study to three dimensions.

Acknowledgements

This research was partly supported by the Canadian Foundation for Climate and Atmospheric Sciences trough a grant to the QPF network and by the Office of Science (BER), U.S. Department of Energy, Grant No. DE-FG02-01ER63199.

References

[1] K.-S. YEH, J. CÔTÉ, S. GRAVEL, A. MÉTHOT, A. PATOINE, M. ROCH, AND A. STANIFORTH, *The CMC-MRB global environmental multiscale (GEM) model: part III - Nonhydrostatic formulation*, Mon. Wea. Rev., 130 (2002), pp. 339–356.

[2] J. CÔTÉ, *A Lagrange multiplier approach for the metric terms of semi-Lagrangian models on the sphere*, Q.J.R. Meteorol. Soc., 114 (1988), pp. 1347–1352.

[3] H.A. SCHWARZ, *Über einen Grenzübergang durch alternirendes Verfahren*, Vierteljahrsschrift der Naturforschenden Gesellschaft in Zürich, 15 (1870), pp. 272–286.

[4] A. QUARTERONI, AND A. VALLI, *Domain Decomposition Methods for Partial Differential Equations*, Oxford Science Publications, 1999.

[5] D.L. WILLIAMSON,J.B. DRAKE, J.J. HACK, R. JAKOB AND P.N. SWARZTRAUBER, *A standard test set for numerical approximations to the shallow water equations in spherical geometry*, J. Comp. Phys., 102 (1992), pp. 211–224.

[6] M.J. GANDER, *Optimized Schwarz Methods*, research report 01-2003, Dept. of Mathematics and Statistics, McGill University, January 2003, to appear in SIAM Journal on Numerical Analysis.

[7] R. JACOB-CHIEN, J.J. HACK, AND D.L. WILLIAMSON, *Spectral transform solutions to shallow water test set* . Comp. Phys., 119 (1995), pp. 164–187.

[8] J. CÔTÉ, M.J. GANDER, L. LAAYOUNI, AND A. QADDOURI, 2006: *Optimized Schwarz methods in spherical geometry with an overset grid system*. Proceedings of the 16th International Conference on Domain Decomposition Methods, New York, USA, January 12-15, 2005. Springer, in print.

[9] J. CÔTÉ, AND A. STANIFORTH, *A two-time-level semi-Lagrangian semi-implicit scheme for spectral models*. Mon. Wea. Rev., 116 (1988), pp. 2003–2012.